Pergamon

PII: S0301-9322(96)00073-0

Int. J. Multiphase Flow Vol. 23, No. 2, pp. 205–226, 1997

0301-9322/97 $17.00 + 0.00

LIQUID TURBULENCE STRUCTURE AT A SHEARED AND WAVY GAS–LIQUID INTERFACE

C. LORENCEZ[1], M. NASR-ESFAHANY[1], M. KAWAJI[1]† and M. OJHA[2]

[1]Department of Chemical Engineering and Applied Chemistry [2]Institute of Biomedical Engineering, University of Toronto, Toronto, Ontario, Canada M5S 3E5

(Received 25 May 1994; in revised form 30 September 1996)

Abstract—Interfacial momentum transfer was studied in cocurrent and countercurrent wavy–stratified flows in a rectangular channel using both the hot-wire anemometry (HWA) and the non-intrusive photochromic dye activation (PDA) techniques. In cocurrent and countercurrent stratified flows with a wavy interface, the interfacial shear and waves were found to change the kinematic and turbulence structures of the liquid phase significantly. In particular, the mean streamwise velocity profile became nearly constant in the upper half of the liquid phase, and the magnitude of the turbulent streamwise and vertical fluctuations correlated with the interfacial shear and the wave amplitude, respectively. Numerical predictions of the experimental data were obtained with the k–ϵ model of turbulence. New interface conditions were proposed for wavy flows which yielded predictions in good agreement with the experimental data for both cocurrent and countercurrent flows. © 1997 Elsevier Science Ltd. All rights reserved.

Key Words: multiphase flow, stratified flow, wavy flow, turbulence, free surface, interfacial shear, photochromic dye activation, hot wire anemometry

1. INTRODUCTION

The interaction between turbulent gas flows and moving liquid streams has been a subject of intense research in the last several decades, due mainly to the importance of transport processes at the gas–liquid interfaces in the chemical industry, and environmental and geophysical sciences. The local structure of turbulence at moving gas–liquid interfaces is an important factor in the transport of mass, momentum and energy between the gas and liquid phases in most two-phase flows. An understanding of the mechanisms which create, convect and diffuse turbulence at moving interfaces is essential as a basis for more accurate mathematical modeling of the interfacial transport processes.

One of the simplest flows with a freely moving surface is a stratified two-phase flow, in which a liquid flows in a horizontal channel and a gas flows over the liquid layer with a smooth or wavy interface separating the phases. The nature of turbulence in stratified or wavy flow in a horizontal channel has been studied in the past by a number of investigators such as Johns *et al.* (1975), Akai *et al.* (1981), Fabre *et al.* (1983, 1987), Murata *et al.* (1991) and Lorencez *et al.* (1991, 1993) among others, however, our understanding of the turbulence structures near a sheared and wavy interface is not yet fully satisfactory.

Through numerous investigations on turbulence structures in single-phase flows, the main phenomena that occur near the solid boundaries have been clarified, and one of the most significant developments in wall turbulence research to data, has been the discovery of organized or coherent structures (e.g. Kline *et al.* 1967; Kim *et al.* 1971; Nakagawa and Nezu 1981; Smith and Metzler 1983; Rashidi and Banerjee 1990), which periodically lift away from the wall, oscillate and then become unstable and break up, resulting in ejection of a substantial portion of the low-speed fluid into the outer flow. The cycle of events, which is conventionally referred to as a turbulent burst, ends with an in-sweep or in-rush of high velocity fluid to replace the ejected fluid in the wall region.

In open channel flows, intense experimental research has been performed over the past 25 years on the mean flow and turbulence structures with Hot Wire or Film Anemometry (HWA) (Nalluri

†To whom all correspondence should be addressed.

and Novak 1977), Laser Doppler Anemometry (LDA) (Nezu and Rodi 1986; Fabre *et al.* 1987) and various visualization methods such as hydrogen-bubble technique (Grass 1971). It has been established through these studies that open channel flows consist of two main regions: an inner region near the wall and an outer region near the free surface. The shear-free surface exercises an influence only on this outer region, and one of the most noticeable effects is the damping of the vertical fluctuations by the surface, which was examined by a number of investigators including Komori *et al.* (1982), and Celik and Rodi (1984). In this configuration, turbulence is generated in a typical burst manner in the vicinity of the viscous sublayer at the bottom wall, as shown by a number of studies (e.g. Komori *et al.* 1988, 1989; Rashidi and Banerjee 1990). More recently, Rashidi *et al.* (1992) examined the wave-turbulence interaction in open channel flows by superimposing two-dimensional waves of different amplitudes and wavelengths on a turbulent open channel flow via a wavemaker. It was shown that the waves increased the frequency of wall ejections, giving rise to an increase in the measured values of turbulence intensities and Reynolds stresses throughout the liquid phase.

In horizontal stratified two-phase flows with a smooth or wavy gas–liquid interface, a mean shear stress is imposed on the liquid surface by a gas flowing either cocurrent or countercurrent to the liquid. Although the flow characteristics such as liquid holdup and pressure drop have been extensively studied, our understanding of the turbulent flow structure in stratified or wavy flow is still quite limited. Rashidi and Banerjee (1990) reported that at high interfacial shear rates, streaks appeared at the smooth interface and broke down to form bursts, as similarly seen at the lower liquid–wall interface.

The details of turbulence structure near the wavy gas–liquid interface in stratified flow are not easy to obtain due to the difficulty in making accurate measurements close to the free and moving interface using conventional instrumentation. The surface can be easily distorted by the presence of a probe, such as a hot-film probe, and the interfacial waves can seriously interfere with the laser beam in LDA measurements. Fabre *et al.* (1987) have presented one of the few successful LDA measurements of turbulence parameters close to the wavy interface for wavy stratified flow. The shortage of experimental data, however, limits the numerical simulation of stratified flows with a wavy interface. Most of the simulations in the earlier studies using a k–ϵ model and different interfacial boundary conditions have produced only a limited success (Akai *et al.* 1981; Benkirane *et al.* 1990; Murata *et al.* 1991; Lorencez *et al.* 1991).

Thus, the main objectives of this work are: (1) to investigate the turbulent flow structure near the gas–liquid interface in cocurrent and countercurrent stratified two-phase flows with a wavy interface, by measuring the streamwise and vertical velocity profiles and their velocity fluctuations near and at the gas–liquid interface; and (2) to use this information to formulate appropriate interfacial boundary conditions for the k–ϵ model, and therefore, improve the mathematical modeling of the near interface region in the liquid phase. In this paper, the experimental work is first described followed by numerical predictions of the experimental results.

2. EXPERIMENTS

2.1. Experimental apparatus

The present study was conducted using a flow loop which included a rectangular flow channel and other components necessary for investigating cocurrent and countercurrent flows, as shown in figure 1. The test channel was formed by three 240 cm sections of a rectangular channel 100 mm wide and 50 mm high internally, which were joined end-to-end by flanges and assembled to ensure that the inside channel walls were flush. The working fluids were air and kerosene (Shell-Sol 715), and the experiments were conducted at near atmospheric pressure and room temperature. A measurement station, including an optical window and hot-film port for the photochromic dye activation method and HWA, was located in the ceiling of the test channel at a sufficient distance, $L = 440$ cm, from the liquid inlet to ensure fully developed flow. Pressure drop was measured in the gas phase using a Baratron differential pressure cell and the liquid level was measured continuously at three locations using parallel wire probes as previously described by Sadatomi *et al.*

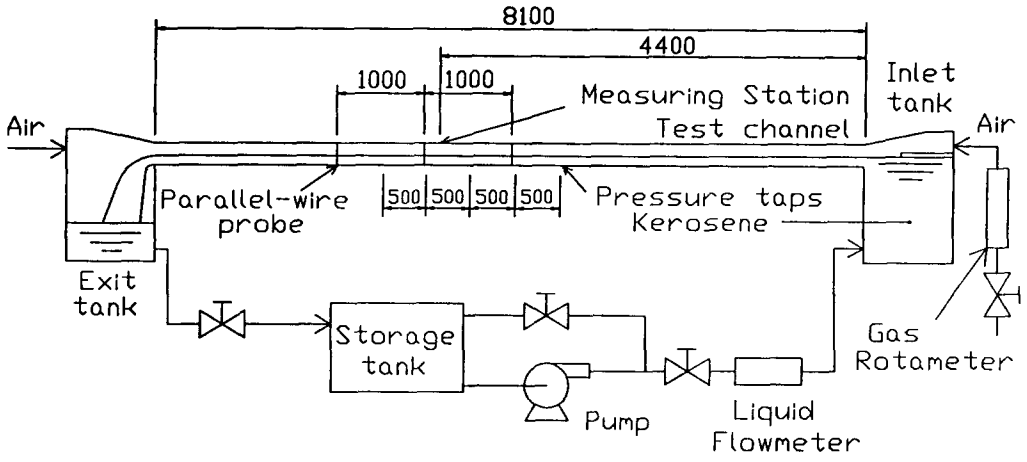

Figure 1. Experimental apparatus.

(1993). Mean liquid level and interfacial level gradient could be obtained from the parallel wire probe data.

2.2. *Photochromic dye activation (PDA) technique*

A non-intrusive photochromic tracer technique was used to visualize the instantaneous motion of the liquid near the interface. A photochromic dye, 1′,3′,3′-trimethylindoline-6-nitrobenzospiropyran (or TNSB), with a short ultraviolet (UV) absorption spectrum and soluble only in organic liquids, was dissolved in dilute concentration in kerosene, a clear liquid. Since its initial development (Popovich and Hummel 1967), the photochromic dye activation technique has been used to investigate a variety of single-phase flow problems (Iribarne *et al.* 1972; Seeley *et al.* 1975, among others). In these earlier studies, only a limited amount of quantitative measurements could be obtained due to various problems. Recent improvements (Ojha *et al.* 1988; Lorencez *et al.* 1993; Kawaji *et al.* 1993) have significantly reduced these shortcomings. Modification of the optics has resulted in sharper and thinner traces, which has improved the overall accuracy in the velocity measurements, especially near the moving gas–liquid interfaces. Detailed error estimates of the velocity and turbulent fluctuation profiles obtained with PDA technique have been provided by Humphrey (1977).

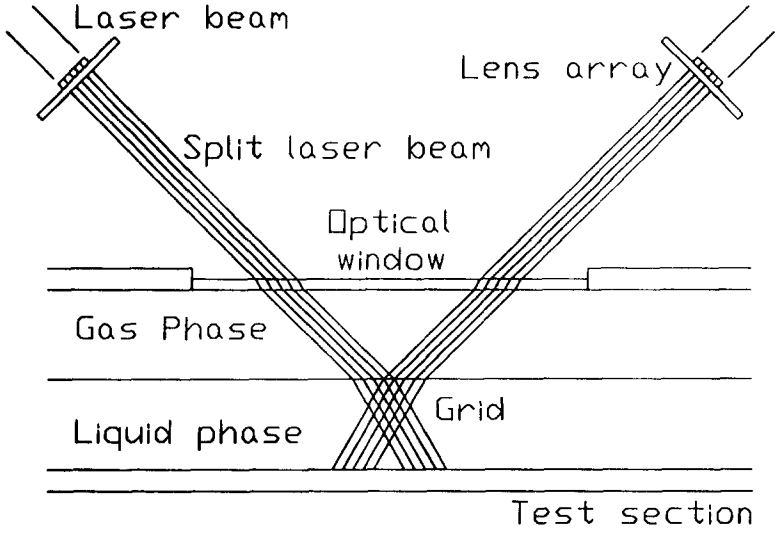

Figure 2. Grid formation using PDA technique.

In the present work, pulsed UV light with a wavelength of 351 nm from an EXCIMER laser (Series TE-860-4 from Lumonics) was focused using two lens arrays with a focal length of 250 mm. Each lens array produced five traces in the photochromic solution, and the two main beams were intersected to form a 5×5 photochromic grid (see figure 2). The traces are formed as the photochromic dye molecules in the path of the laser beam are activated and a dark color appears in the liquid containing the activated dye molecules. The concentration of the dye in the liquid can be adjusted to optimize the penetration depth of the UV light beam and the contrast of the traces formed. The best results were obtained with a dye concentration of approximately 0.01% by weight. The optical system was adjusted to create narrow, sharp intersecting traces in the liquid (see figure 3). Care was taken to ensure that the traces were formed at the central vertical plane to be viewed from the side of the test section.

The motion of the traces in the liquid phase was recorded with a PHOTRON digital high speed video camera system, which was positioned horizontally facing the side of the channel and inclined slightly upward (8°) to view the traces from below the interface, in order to overcome optical obstruction by the surface waves when viewed normal to the test section. The arrangement allowed accurate determination of the interface position and shape at the plane of the trace formation since the liquid surface acted as a mirror and reflected the trace images as shown in figure 3. The digital data stored in the high speed video camera system were first transferred to a Super-VHS video tape using a Panasonic VCR Model AG-7355, which has a digital frame freeze feature for jitter-free transfer of a frame to a microcomputer-based image analysis system.

From the displacement of the grid pattern, the velocities of the grid points in x and y directions were calculated, which is a significant improvement over the use of non-intersecting traces

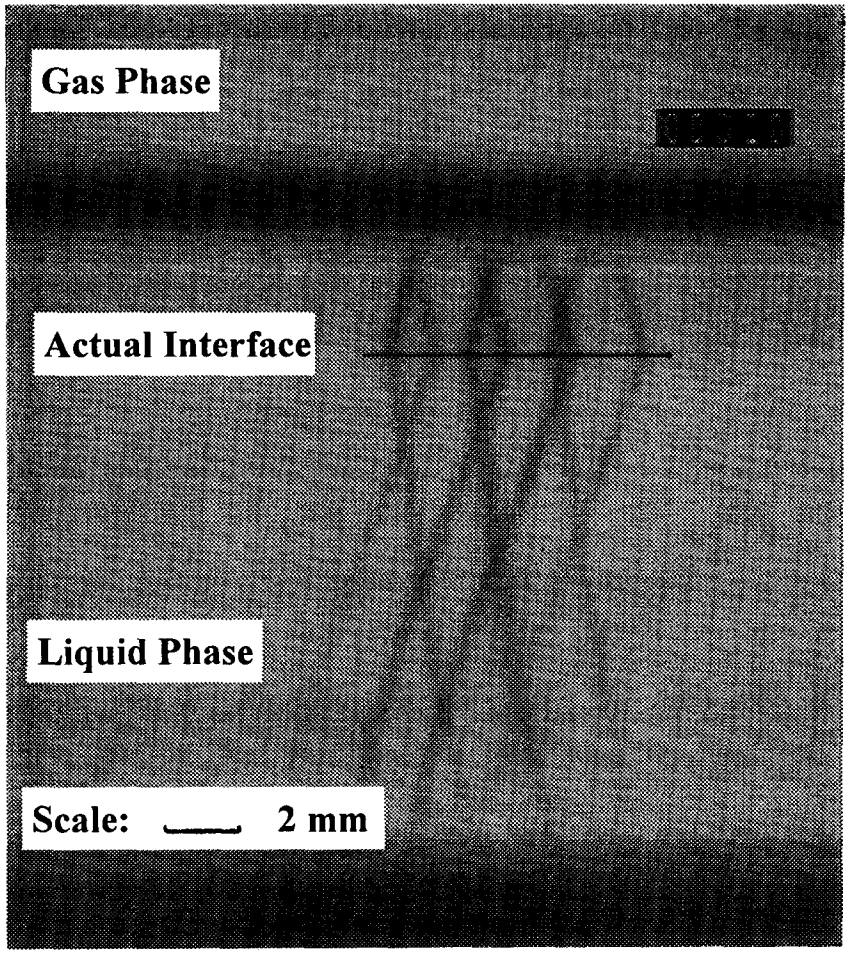

Figure 3. Grid pattern formed with PDA technique.

previously used by the authors (Lorencez *et al.* 1991) to obtain only the streamwise velocity profiles in smooth interface flows. Additional information was obtained from the grid pattern by dividing the length of each trace segment located between two adjacent grid points into N equal portions yielding $N + 1$ points, including the grid points. Assuming that these $N + 1$ points moved into the corresponding $N + 1$ points along the same trace segment of the next frame, streamwise and vertical velocities were obtained for these interpolated points. Here, $N = 5$ yielded detailed enough velocity profiles.

The accuracy achieved in the calculation of the velocity profiles was satisfactory. For example, it was estimated (Lorencez 1994) that in the calculations of instantaneous velocity profiles of a liquid stream with a turbulence intensity of 0.15, the relative error involved using this method was 2.5%. This error is a direct consequence of the limited spatial resolution of the image analysis system used.

2.3. *Hot-wire anemometry*

In addition to the photochromic dye activation method described above, a two-channel hot-film anemometer (Dantec 5601 and 56C17 bridges) with a cross-wire film probe (Dantec 55R63) was used to measure the velocity profiles in both liquid and gas phases. Two differential input channels were simultaneously sampled at a rate of 1 kHz/channel for 60 s. A separate flow loop was used to calibrate the hot-film probe for air. Calibration of the hot-film probe in kerosene at low velocities was performed using a slight variation of the method proposed by Hirano *et al.* (1989). Data sampling was performed using a digital data acquisition system installed in a microcomputer.

2.4. *Experimental conditions*

In order to study the flow structure near the gas–liquid interface, five different cases were examined: open channel flow, and cocurrent and countercurrent flows with a wavy interface, at a constant liquid volumetric flow rate. The experimental conditions are summarized in table 1, which includes the volumetric flow rates, Q_L and Q_G, pressure drop, Δp, mean liquid height, h_L, wave amplitude, Δh, wave period, T, liquid wall friction velocity, u_{*WL}, interfacial gas friction velocity, u_{*iG}, liquid and gas Reynolds numbers, Re_L and Re_G, and the type of flow. The wave amplitude, Δh, represents the rms value of the variations in the liquid height. The interfacial waves were not random but periodic having a certain dominant frequency.

The determination of the interfacial shear stress and its corresponding interfacial gas friction velocity, u_{*iG}, was accomplished following the method suggested by Sadatomi *et al.* (1993). This method involves a momentum balance in the gas phase, in which the four most important contributions are considered: the pressure drop, the wall shear stress, the interfacial level gradient and the interfacial friction. Once the first three terms are evaluated from experimental measurements, the momentum balance is solved for the interfacial shear stress. The Reynolds number was computed in terms of the hydraulic diameter for each phase, and the wall friction velocity was obtained by fitting the streamwise velocity profile data to the universal velocity profile.

The details of the measurement techniques, uncertainty analyses, image processing and data reduction procedures are given in Lorencez (1994).

3. EXPERIMENTAL RESULTS AND DISCUSSION

To study the kinematic structure of the liquid flow, accurate and detailed velocity profiles were obtained using both the HWA and PDA techniques. In particular, the structure of the top layers

Table 1. Experimental conditions

Run	$Q_L \times 10^4$ (m^3/s)	$Q_G \times 10^2$ (m^3/s)	$\Delta p/\Delta x$ (Pa/m)	h_L (mm)	Δh (mm)	T (sec)	u_{*WL} (cm/s)	u_{*iG} (cm/s)	Re_L	Re_G	Case
100	3.8	0	0	17.2	0.24	—	1.10	0	6000	0	Open channel
200	3.8	1.1	−3.16	16.7	0.67	0.09	1.77	24.7	6010	10690	Cocurrent
300	3.8	1.8	−10.1	14.3	1.62	0.14	2.71	43.3	6250	17200	Cocurrent
400	3.8	0.52	−1.57	18.1	0.68	0.64	1.32	11.6	5900	5020	Countercurrent
500	3.8	0.80	−3.50	18.7	1.56	0.52	1.27	15.9	5840	7170	Countercurrent

of the liquid was investigated without disturbing the liquid interface by using the photochromic method. Although the kinematic and turbulence structures of the gas phase were also obtained with HWA, they will not be presented in depth in this paper since they can be found elsewhere (Lorencez 1994; Lorencez *et al.* 1991) and the main objective here is to report on the turbulence structure in the liquid phase near a wavy gas–liquid interface. Only the mean velocity profiles, turbulence intensities and their numerical predictions for the gas phase will be briefly presented in this paper.

3.1. Instantaneous flow characteristics

In earlier experiments (Lorencez *et al.* 1991), laminar and turbulent open channel flows were studied with multiple non-intersecting traces. In the laminar case, the traces adopted a parabolic shape after their formation in the liquid phase and no disturbance was observed as shown in figure 4. In contrast to this, the traces formed in the turbulent open channel flow were almost immediately deformed as previously observed by Rashidi and Banerjee (1990) as a consequence of the velocity fluctuations generated by the turbulent bursts created near the lower wall region and moving towards the bulk of the liquid, as shown in figure 5. The grid traces in cocurrent and countercurrent two-phase flow with a wavy interface were also affected by these disturbances and showed subsequent deformations resulting in unusual instantaneous velocity profiles, as pointed out by Hewitt (1991). The deformation of the traces in wavy flow is due not only to the turbulent bursts generated at the lower wall, but also to interfacial turbulent bursts created by the interaction of the waves and the gas flow. Video images recorded using PDA showed that this interaction causes an axially non-uniform interfacial shear acting on the wavy liquid surface. In cocurrent flow, the shear accelerated the near interface region of the liquid to a velocity considerably greater than

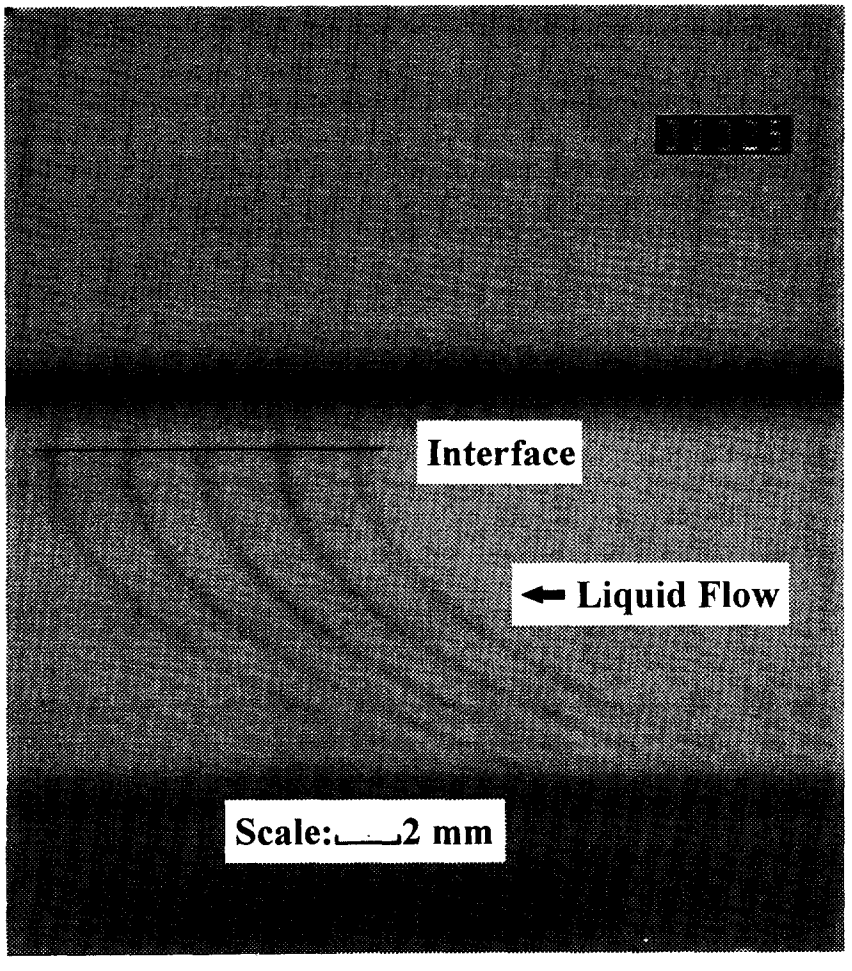

Figure 4. Parallel photochromic traces formed in laminar open channel flow.

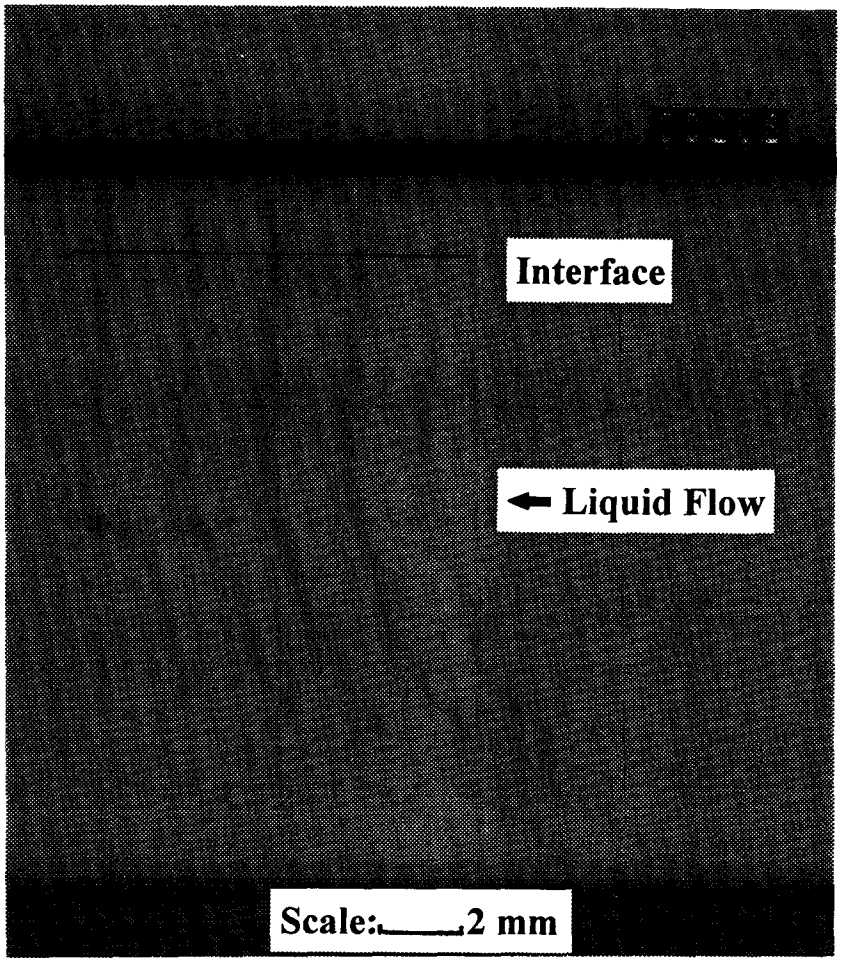

Figure 5. Parallel photochromic traces formed in turbulent open channel flow.

the mean liquid velocity on the windward side of the wave, and slowed it down to near the mean liquid velocity on the leeward side of the wave, as shown in figures 6 and 7, respectively. Exactly the opposite effect was observed in countercurrent flow. In both cases, it was clearly seen from the video images that turbulent bursts generated on the windward sides of the waves traveled from the wavy region towards the lower wall, in a manner similar to the ejections from the wall moving towards the interface. Also, the number of turbulent bursts increased in proportion to the increases in gas flow rates and roughness of the interface.

This suggests that a mechanism of momentum transport from the gas flow towards the liquid stream in stratified two-phase flow is mainly through the generation of these interfacial turbulent bursts (high momentum-carrying lumps of liquid) as a result of the interaction between the gas flow and liquid waves. Then, the interfacial turbulent bursts move from the upper layers towards the bulk of the liquid increasing the mixing motion in the fluid, i.e. increasing the turbulent velocity fluctuations and their correlations near the interface, improving the scalar transport between the two phases.

Although the instantaneous velocity profiles appeared to be highly distorted at times, they yielded reasonable kinematic and turbulence data when the time-mean velocity profiles were calculated, as discussed below.

3.2. Time-averaged flow characteristics

The presence of the two-phase region (wavy region) required the application of phasic averaging to obtain the time-averaged flow characteristics. A minimum of 150 velocity profiles were analyzed for this region. On the other hand, it was found that in the bulk of the liquid the analysis of 100

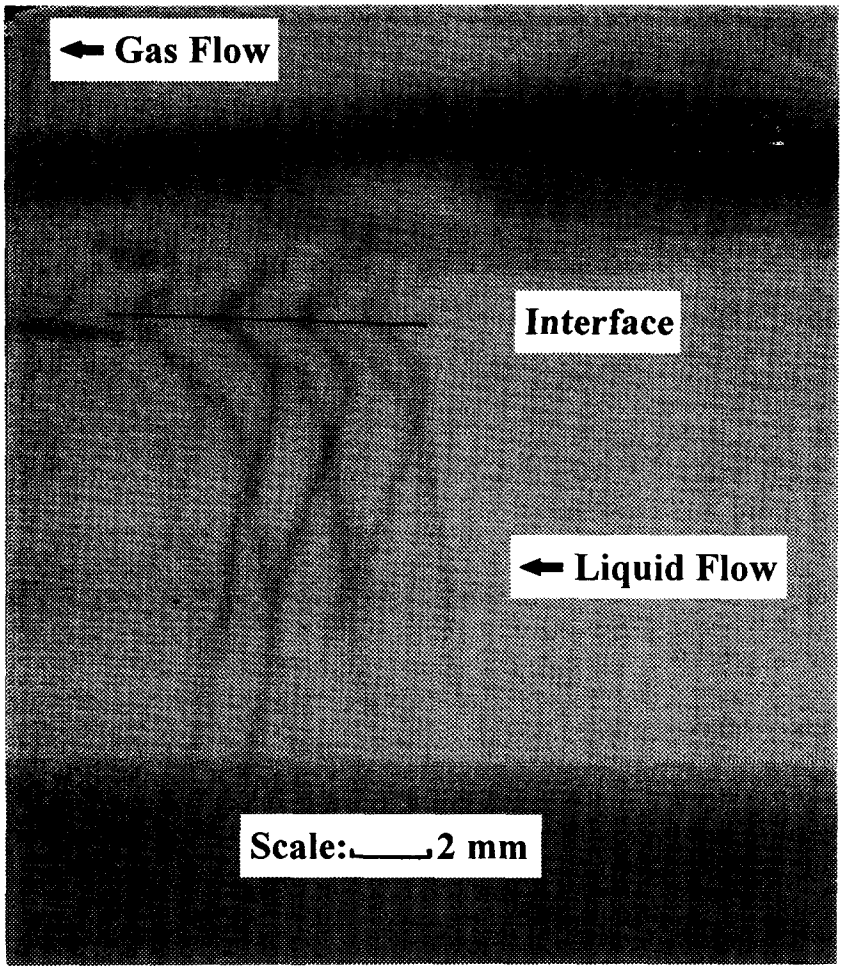

Figure 6. Photochromic traces formed on the windward side of the wave.

profiles yielded good statistics. The dimensional streamwise mean velocity profiles for the different experimental conditions are shown in figure 8, where the error bars represent the standard deviation of the data from the mean. Run 100 was in the turbulent regime and although not shown here, its streamwise mean velocity profile followed closely the universal velocity profile for turbulent flow when plotted in dimensionless coordinates (Lorencez 1994). For each flow condition, the data obtained with both HWA and PDA techniques agreed well in the overlapping region and together they provided a detailed description of the mean velocity profile in the entire liquid up to the gas–liquid interface.

To examine the effects of cocurrent gas flow, Runs 200 and 300 were conducted with an increasing volumetric gas flow. It was found that the gas flow imposed a strong interfacial shear upon the liquid layer, inducing a wavy interface which modified the kinematic structure in the liquid phase compared to that of Run 100. The flow in Run 200 resembled a Couette-type flow where the plane of the maximum velocity is found at the interface. However, a significant difference was observed in the kinematic structure of Run 300, where a rather flat mean streamwise velocity profile was measured in the bulk liquid, and only the layers close to the interface were moving slightly faster. The flat mean velocity profile is possibly a result of the enhanced vertical mixing due to the presence of larger waves, where the flatness of the streamwise velocity profiles was observed to increase as the wave amplitude increased (Lorencez 1994).

Also, to examine the effects of countercurrent gas flow, Runs 400 and 500 were conducted with an increasing gas flow. The plane of the maximum velocity was always positioned just underneath the gas–liquid interface, as a result of the opposing interfacial shear imposed by the gas flow. The

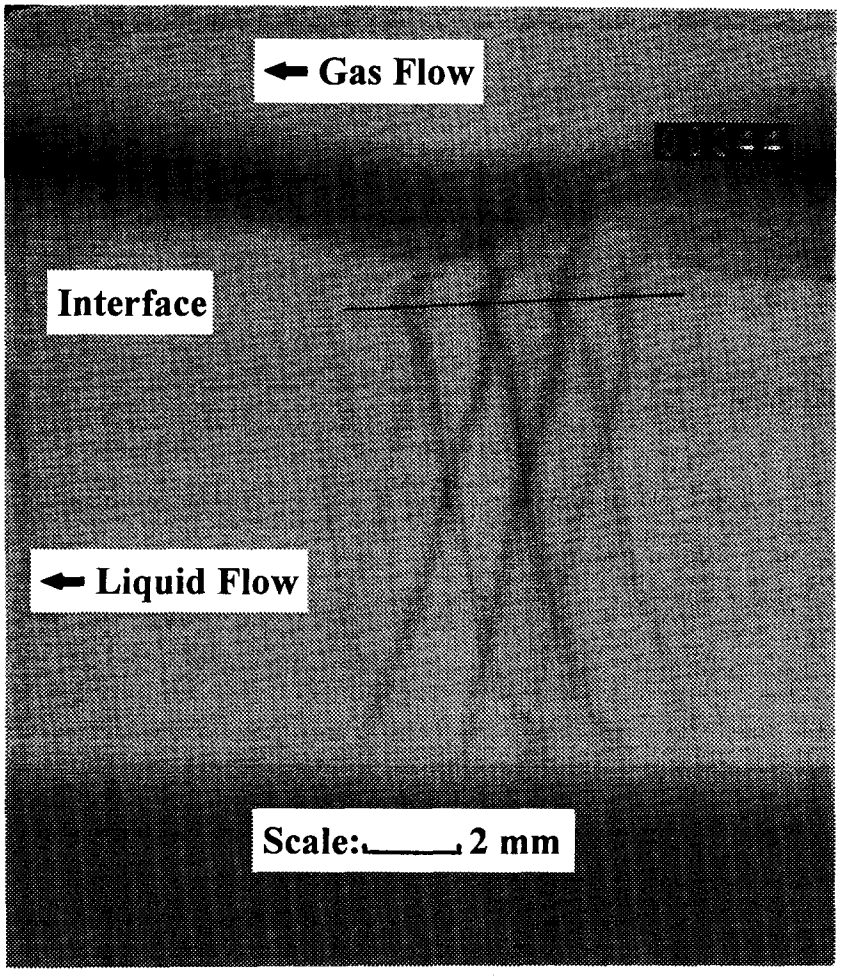

Figure 7. Photochromic traces formed on the leeward side of the wave.

overall effect of the resulting interfacial shear was retardation of the liquid flow causing an increase in the mean liquid height. This retardation effect on the liquid flow was mostly noticed in the top layers of the liquid phase.

The vertical mean velocity profiles for the different experiment conditions are shown in figure 9. Vertical velocities with a magnitude of up to about 6% of the mean streamwise velocity were observed in every run. In all cases, the vertical motion was damped by the channel floor and the gas–liquid interface as measured by the hot-film probe and the photochromic tracer, respectively. Similar vertical motion has also been observed in cocurrent stratified flow in a rectangular channel by Fabre *et al.* (1983).

Concerning the measurements of the turbulence field, the streamwise and vertical velocity fluctuations as well as the Reynolds stress profiles normalized with the wall friction velocity for each experimental run are plotted against the height normalized with the mean liquid layer thickness, y/h_L, in figures 10–12, respectively.

In Run 100, the streamwise velocity fluctuations (figure 10) reached a maximum value near the lower wall and monotonically decreased when approaching the smooth interface, but did not vanish at the interface. In contrast, the vertical fluctuations (figure 11) were damped both at the lower wall and the gas–liquid interface and their amplitude was smaller than that of the streamwise velocity fluctuations. The Reynolds stress profile for the same run (figure 12) reached its maximum near the wall and vanished at the interface.

The turbulence fields and Reynolds stress profiles in cocurrent and countercurrent wavy flows for the other flow conditions are also shown in figures 10–12. The turbulence structure of the liquid

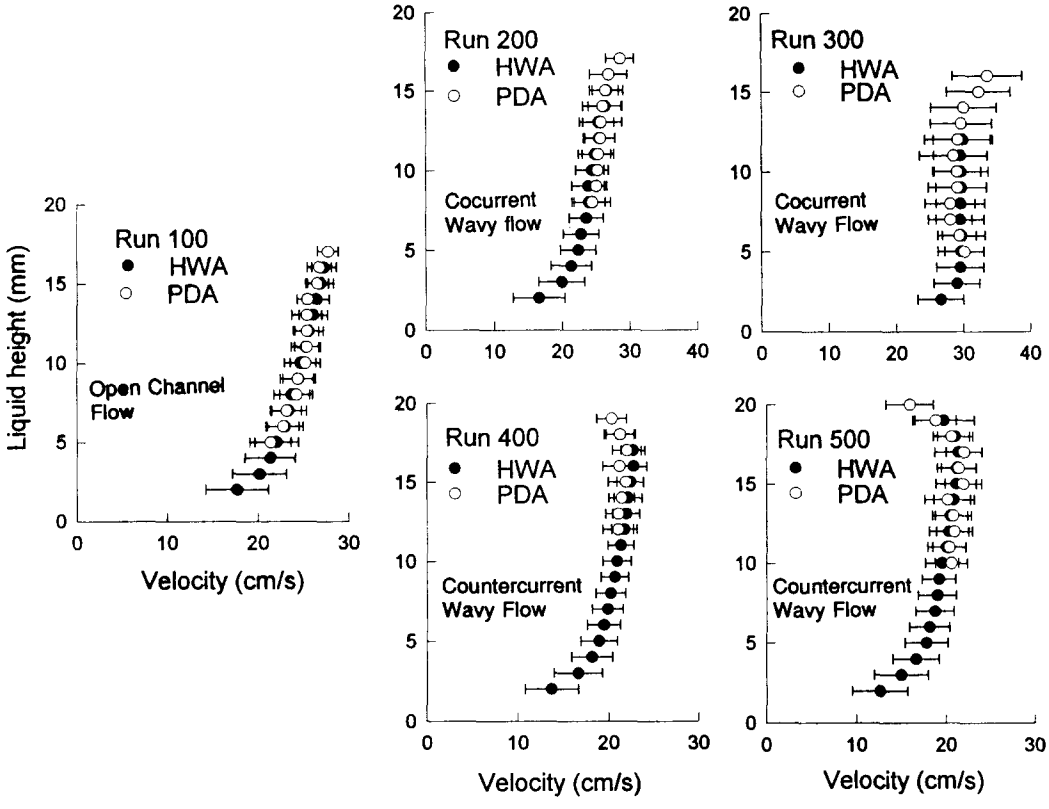

Figure 8. Streamwise velocity profiles obtained with HWA and PDA techniques.

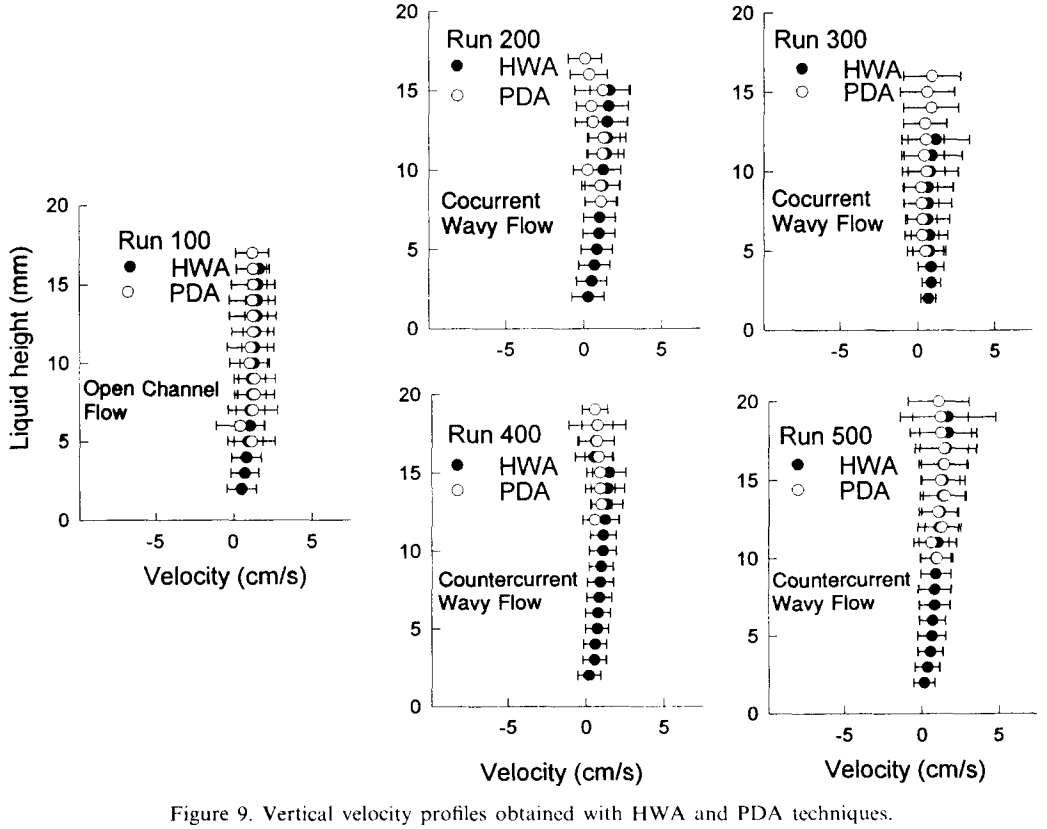

Figure 9. Vertical velocity profiles obtained with HWA and PDA techniques.

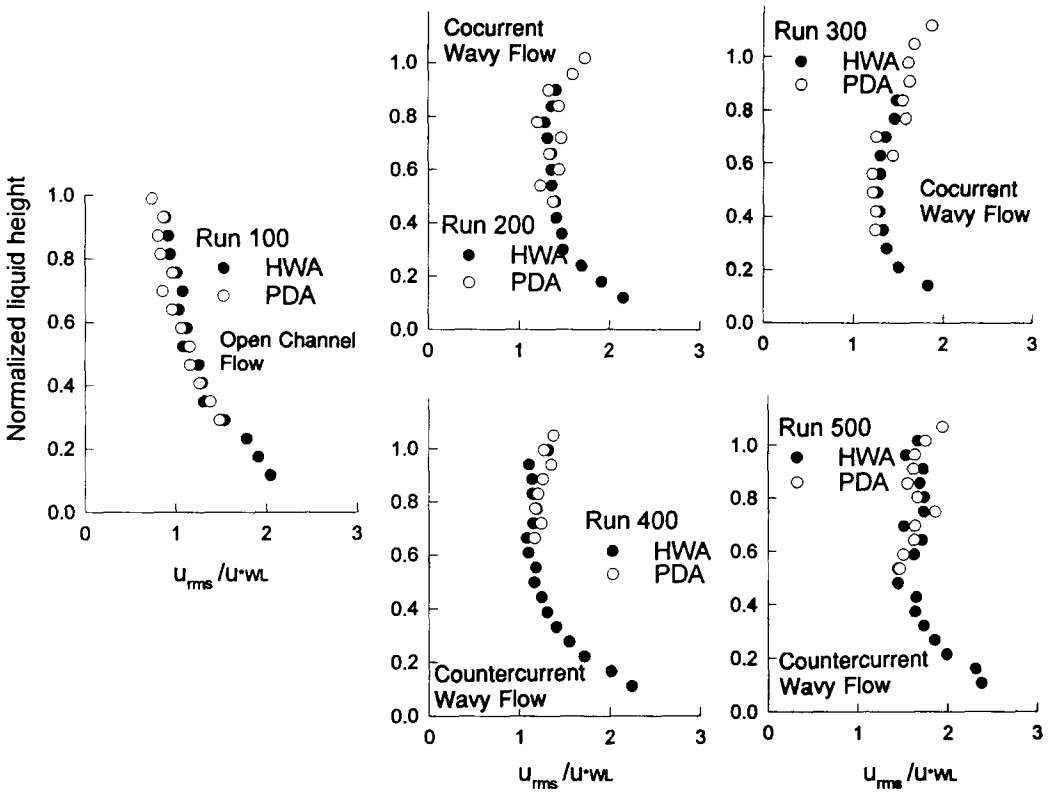

Figure 10. Streamwise velocity fluctuation profiles obtained with HWA and PDA techniques.

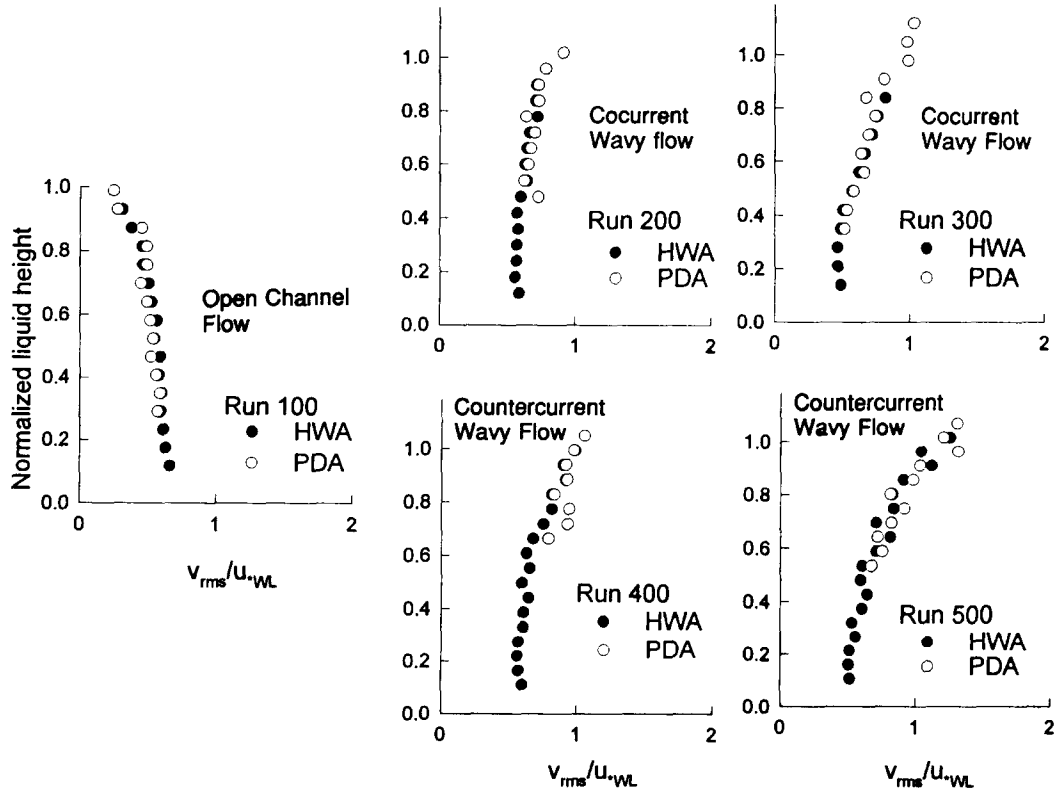

Figure 11. Vertical velocity fluctuation profiles obtained with HWA and PDA techniques.

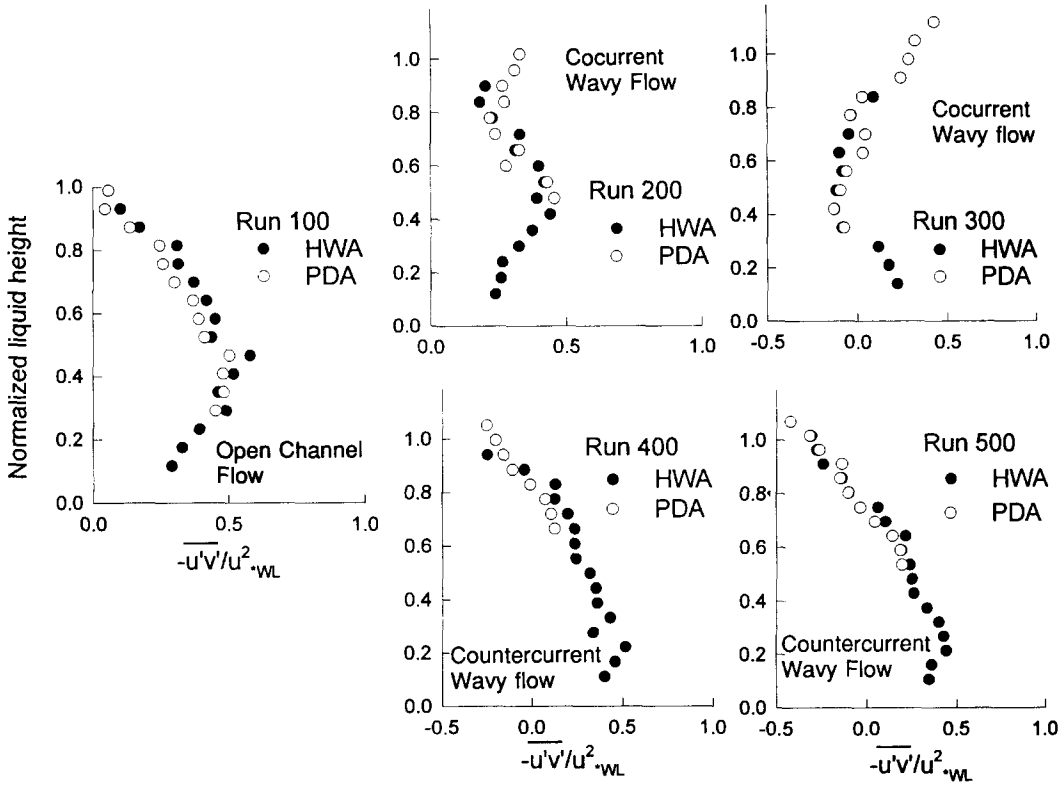

Figure 12. Reynolds stress profiles obtained with HWA and PDA techniques.

phase with a wavy interface was notably modified as compared to that with a smooth interface. In particular, it seemed that the axially non-uniform shear enhances the streamwise fluctuations near the gas–liquid interface primarily by the acceleration/deceleration cycles described earlier. It is clear from figure 10 that the value of u' near the interface increases in proportion to the increments in the interfacial shear, for both cocurrent and countercurrent flow. Concerning the vertical fluctuations shown in figure 11, it was found that when interfacial waves appeared along the interface the amplitude of the vertical fluctuations did not decrease towards zero in the neighborhood of the interface as it did in an open channel flow, but increased markedly near the interface due to the waves. The additional data obtained by Lorencez (1994) show a clear change in the profile of v' from that of a continuous decrease from the wall towards the interface, to that of a continuous increase. This is due to the increased contribution of the vertical motion of the interfacial waves as the waves grow in amplitude and frequency with the increase in the gas flow rate. It is not that the amplitude of the vertical velocity fluctuations decreases near the bottom wall from their normal values existing in a corresponding open channel flow, but it increases at all values of y as is clear from figure 11 showing the rms of v' normalized with the wall friction velocity which increases with the interfacial wave amplitude as listed in table 1. Thus, in both cocurrent and countercurrent flows, the velocity fluctuations reached the largest magnitudes near the wavy gas–liquid interface.

The Reynolds stress values of Run 100 (figure 12) decreased to zero as the interface was approached because of the damping of the vertical turbulent fluctuations by the smooth gas–liquid interface. For the wavy cocurrent and countercurrent flows, the presence of waves enhanced the vertical velocity fluctuations near the interface and the Reynolds stress profiles did not vanish at the interface and were considerably modified as compared to the linear profiles of open channel flows. The profiles for cocurrent and countercurrent flows show that the wavy region produces fluxes of Reynolds stress comparable to those from the wall, mainly through the enhanced mixing

caused by the interfacial turbulent bursts in the upper layers of the liquid. To understand the modification in the Reynolds stress profile for wavy flows, it should be kept in mind that for the case of cocurrent flows the maximum velocity is reached at the gas–liquid interface. Therefore, the turbulent bursts generated at the interface traveled towards the lower wall ($v' < 0$) giving rise to a positive component ($u' > 0$) in the streamwise velocity. Thus, the time-average value of the product $-u'v'$ is positive, as seen in figure 12 for Runs 200 and 300. For the countercurrent case, the maximum velocity is not reached at the gas–liquid interface but at a plane below the interface due to the retardation effect of the gas flow. Then, the turbulent bursts generated at the interface and moving downwards ($v' < 0$) give rise to a negative component ($u' < 0$) in the streamwise velocity. In this case, the time-average value of the product $-u'v'$ is negative, as seen in figure 12 for Runs 400 and 500.

More research needs to be done to further clarify whether the Reynolds stress profile for cocurrent and countercurrent wavy flows is simply a superposition of the Reynolds stress fluxes generated at both boundaries or involves a much more complex interaction.

4. NUMERICAL PREDICTION OF EXPERIMENTAL RESULTS

The k–ϵ model of turbulence was chosen to predict the kinematic and turbulence fields reported here, because it has been the most widely used and best tested of all the two-equation models of turbulence. Although the k–ϵ model was originally developed for single-phase flows, it has been used to solve some free surface problems by modifying the boundary conditions at the gas–liquid interface (Akai *et al.* 1981; Celik and Rodi 1984; Issa 1988; Benkirane *et al.* 1990; Murata *et al.* 1991; and Lorencez *et al.* 1991). A lack of accurate knowledge about the turbulence structure near the gas–liquid interface, however, has prevented formulation of appropriate interfacial boundary conditions, which explains why few studies of free surface, turbulent flow problems have been conducted with this model.

4.1. Governing equations

The governing momentum equation for fully developed flow of each phase in a horizontal channel is given by

$$\frac{\partial}{\partial y}\left(\nu \frac{\partial u}{\partial y}\right) + \frac{\partial}{\partial z}\left(\nu \frac{\partial u}{\partial z}\right) - \frac{1}{\rho}\frac{\partial p}{\partial x} = 0 \qquad [1]$$

where u is the velocity, ρ is the density, $\partial p/\partial x$ is the pressure gradient in the streamwise direction, and y and z are the vertical and spanwise coordinates. The parameter, ν, is the effective kinematic viscosity which is defined as the sum of the molecular viscosity, ν_m, and the turbulent contribution, ν_T. In this work, two forms of the k–ϵ model were used. The first is the standard version originally formulated for high Reynolds number flows, and used here for $\mathrm{Re} > 10^4$, while the second includes the modifications proposed by Akai *et al.* (1981) for low Reynolds number flows, $\mathrm{Re} \leqslant 10^4$.

For both models, the equations governing the turbulence kinetic energy, k, and its dissipation rate, ϵ, are

$$\frac{\partial}{\partial y}\left(\nu \frac{\partial k}{\partial y}\right) + \frac{\partial}{\partial z}\left(\nu \frac{\partial k}{\partial z}\right) + P - \epsilon = 0 \qquad [2]$$

and

$$\frac{\partial}{\partial y}\left(\nu_\epsilon \frac{\partial \epsilon}{\partial y}\right) + \frac{\partial}{\partial z}\left(\nu_\epsilon \frac{\partial \epsilon}{\partial z}\right) + \frac{\epsilon}{k}\left(f_1 C_1 P - f_2 C_2 \epsilon\right) + B = 0 \qquad [3]$$

The term B is dependent on the version of the turbulence model used. For the low Reynolds number model, Akai *et al.* (1981) proposed the following expression.

$$B = 2f_2C_2\nu\frac{\epsilon}{k}\left[\left(\frac{\partial\sqrt{k}}{\partial y}\right)^2 + \left(\frac{\partial\sqrt{k}}{\partial z}\right)^2\right] + 2\nu\nu_m(\nabla^2 u)^2. \quad [4]$$

When the high Reynolds number model is used, $B = 0$. In both cases, the production term, P, is given by

$$P = \nu_T\left[\left(\frac{\partial u}{\partial y}\right)^2 + \left(\frac{\partial u}{\partial z}\right)^2\right]. \quad [5]$$

The effective diffusion coefficient for the dissipation rate, ν_ϵ, is obtained from

$$\nu_\epsilon = \nu_m + \frac{\nu_T}{\sigma_\epsilon}, \quad [6]$$

and the turbulent viscosity, ν_T, is related to k and ϵ according to

$$\nu_T = C_\mu f_\mu \frac{k^2}{\epsilon}, \quad [7]$$

where the values of the coefficients C_μ and f_μ, as well as C_1, C_2, f_1, f_2 and σ_ϵ are all given in table 2. For the low Reynolds number model, the coefficients f_2 and f_μ are functions of the turbulent Reynolds number, $\mathrm{Re_T}$, which is defined as

$$\mathrm{Re_T} = \frac{k^2}{\nu_m\epsilon}. \quad [8]$$

Equations [1]–[3] must be solved for u, k and ϵ for both phases. Two more unknowns are the pressure gradient, $\partial p/\partial x$, and the mean liquid height, h_L. To close the set of equations, two additional equations are required

$$\int_{A_L} u\,\mathrm{d}A = Q_L, \quad [9]$$

$$\int_{A_G} u\,\mathrm{d}A = Q_G, \quad [10]$$

where A is the phase cross-sectional area, Q is the volumetric flow rate, and subscripts L and G indicate liquid and gas, respectively.

Table 2. Values for the turbulence model coefficients

Coefficient	High Re model	Low Re model
C_1	1.44	1.45
C_2	1.92	2.0
f_1	1.0	1.0
f_2	1.0	$1\ 0.3\exp(-\mathrm{Re_T^2})$
f_μ	1.0	$\exp[-2.5/(1 + \mathrm{Re_T}/50)]$
C_μ	0.09	0.09
σ_ϵ	1.3	1.3

Table 3. Liquid boundary conditions at the wall

Open channel flow Cocurrent flow Countercurrent flow	$u_{wL} = 0$	$k_{wL} = 0$	$\epsilon_{wL} = 2\nu_m\left(\frac{\partial\sqrt{k_{wL}}}{\partial y}\right)^2$

4.2. *Boundary conditions*

At the wall, the boundary conditions for u, k and ϵ, are listed in table 3. Both, u and k must vanish at the solid wall, and ϵ is evaluated from the profile of k near the wall (Akai *et al.* 1981).

The interfacial boundary conditions for u, k and ϵ for an open channel flow listed in table 4, have been previously proposed by Celik and Rodi (1984). In particular, the boundary condition for ϵ

$$\epsilon = \frac{k_{iL}^{3/2}}{a\, h_L} \qquad [11]$$

ensures the reduction of the length scale to, $L \propto k^{3/2}/\epsilon$, and also $\nu_T \propto k^2/\epsilon$ near the gas–liquid interface. The same boundary condition for the dissipation rate, ϵ, was adopted in this work. The value of the constant of proportionality, a, is adjustable, in order to match the experimental level of turbulence (Celik and Rodi 1984). In this work, the chosen value of a was 0.2 for flows with wavy interfaces. Other interfacial boundary conditions for ϵ proposed in previous studies, such as

$$\nabla\epsilon_{iL} = 0 \quad \text{or} \quad \epsilon_{iL} = 2\nu_m\left(\frac{\partial\sqrt{k_{iL}}}{\partial y}\right)^2 \qquad [12]$$

were avoided since the former is a symmetry condition for single-phase flow, and the latter only applies to a solid wall.

In cocurrent and countercurrent flows, the continuity of the velocity field at the interface is required, i.e. $u_L + \Delta u = u_G$, where Δu is the velocity difference across the wavy region and is obtained by applying the wall functions on the gas side of the wavy interface. With respect to the turbulence field, the turbulence kinetic energy (TKE) must have a finite value at the gas–liquid interface as a boundary condition, i.e. $k_{iL} > 0$, since the velocity fluctuations do not vanish at the interface. Some investigators (Benkirane *et al.* 1990; Lorencez *et al.* 1991) have previously suggested $\partial k_{iL}/\partial y = 0$ as a possible boundary condition for the TKE at a wavy interface, but the present and previous experimental data clearly show that TKE increases towards the interface and the slope is not equal to zero. Here, it is proposed that the value of TKE on the liquid side of the interface be given by the contributions from the streamwise and vertical fluctuations

$$k_{iL} = k_U + k_V > 0. \qquad [13]$$

The contribution to TKE from the streamwise fluctuations at the interface was chosen to be proportional to the interfacial shear stress, because the increase in interfacial shear promotes mostly the growth of the streamwise fluctuations when the interface is smooth and the vertical fluctuations are damped

$$k_U = \left(\frac{\rho G}{\rho_L}\right)u_{iG}^2. \qquad [14]$$

Table 4. Liquid boundary conditions at the gas–liquid interface

Open channel flow	$\nabla u_L = 0$	$\nabla u_L = 0$	$\epsilon_L = k_L^{3/2}/ah_L$
Cocurrent and Countercurrent flow	$u_L + \Delta u = u_G$	$k_L = k_U + k_V$	$\epsilon_L = k_L^{3/2}/ah_L$

In cocurrent and countercurrent wavy flows, the streamwise velocity fluctuations also increased with the wavy amplitude of the liquid surface. Here, the large gas velocity imposes greater shear on the liquid surface and due to the non-uniform distribution of the shear stress on the windward and leeward sides of the waves, the streamwise velocity fluctuations are further enhanced compared to the smooth interface case. Thus, the increase in streamwise velocity fluctuations in wavy flow is believed to be a direct result of the increased axially non-uniform interfacial shear rather than the bulk liquid motion induced by the waves. The contribution to TKE from the increased streamwise velocity fluctuations in wavy flow, then, is again given by [14].

In wavy flows, the vertical velocity fluctuations are not damped and increase with the wave amplitude which also increases the interfacial shear stress. However, Rashidi *et al.* (1992) showed that in open channel flows with artificially created waves on the liquid surface but negligible interfacial shear, the magnitude of the vertical velocity fluctuations was increased and it appeared to be larger near the interface than near the wall. This suggests that the effect of the surface waves without any interfacial shear imposed by the gas is to enhance the TKE by increasing the magnitude of all turbulent velocity fluctuations with a preference for the vertical ones. The correlation between the vertical fluctuations and the wave amplitude suggested that k_V could be evaluated from the wave structures in a manner similar to that previously proposed by Akai *et al.* (1981)

$$k_V = \left(\frac{2\Delta h}{T}\right)^2 \qquad [15]$$

where Δh and T are the mean (rms) wave amplitude and wave period, respectively. In the present calculations, experimental values of Δh and T were used. The mean wave amplitude was obtained from the liquid level readings, and the wave period from the high speed video camera recordings.

4.3. *Method of solution*

In this work, the solution domain was discretized into a finite number of rectangular cells of variable size in each phase, and the governing equations were discretized by integration of these

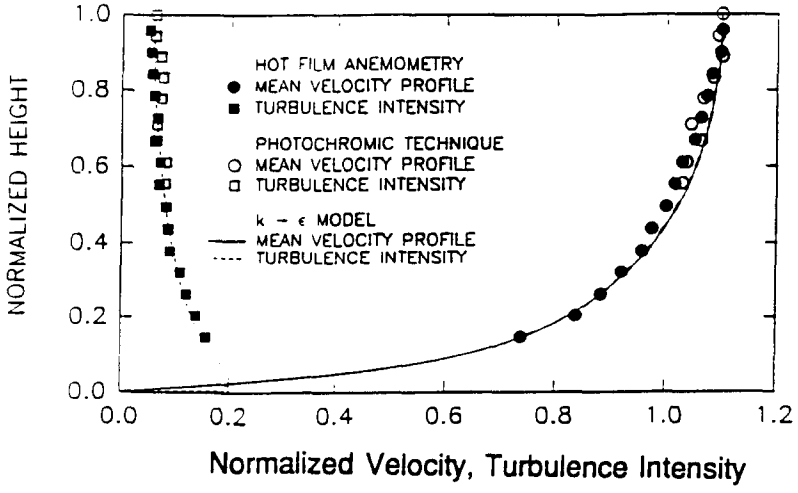

Figure 13. Normalized streamwise velocity and turbulence intensity profiles in open channel flow for Run 100.

equations over the cells. There were 50 cells in each phase in the vertical direction of 20 in the lateral direction. Further addition of computational cells had only a slight effect on the final results; thus, a grid-independent solution was ensured. The equations were solved iteratively by using the Semi-Implicit Method for Pressure Linked Equations Revised (SIMPLER) algorithm (Patankar 1980), with the boundary conditions for the liquid phase at the wall and at the gas–liquid interface listed in tables 3 and 4, respectively.

The cycle of calculations starts with guessed values of u, k and ϵ in each phase as well as the mean liquid height, h_L. Then the continuity and momentum equations are solved using the SIMPLER algorithm and the boundary conditions to yield the new velocity field, u, for each phase. The mean liquid height is then computed from the average liquid velocity, the liquid volumetric flow rate and the width of the channel. The k and ϵ fields are computed next from their own transport equations. This calculation cycle is repeated until convergence is attained, e.g. when the mass source term is smaller than a given tolerance.

For the present numerical calculations, the density and kinematic viscosity of air used were 1.18 kg/m^3 and 1.57×10^{-5} m^2/s, respectively, and those for kerosene were 755 kg/m^3 and 1.87×10^{-6} m^2/s.

4.4. *Comparison of predictions with data*

The numerical predictions of the kinematic and turbulence fields in the liquid phase are shown in figures 13–17, for open channel flow, and cocurrent and countercurrent flows. Plotted in these figures are the measured and predicted values of streamwise velocity profiles, normalized with the liquid velocity at the position, $y/h_L = 0.5$, for each experimental run, as well as the experimental and theoretical turbulence intensity profiles. For the gas phase, the velocity profile was normalized with the maximum velocity and the results are shown in figures 14–17.

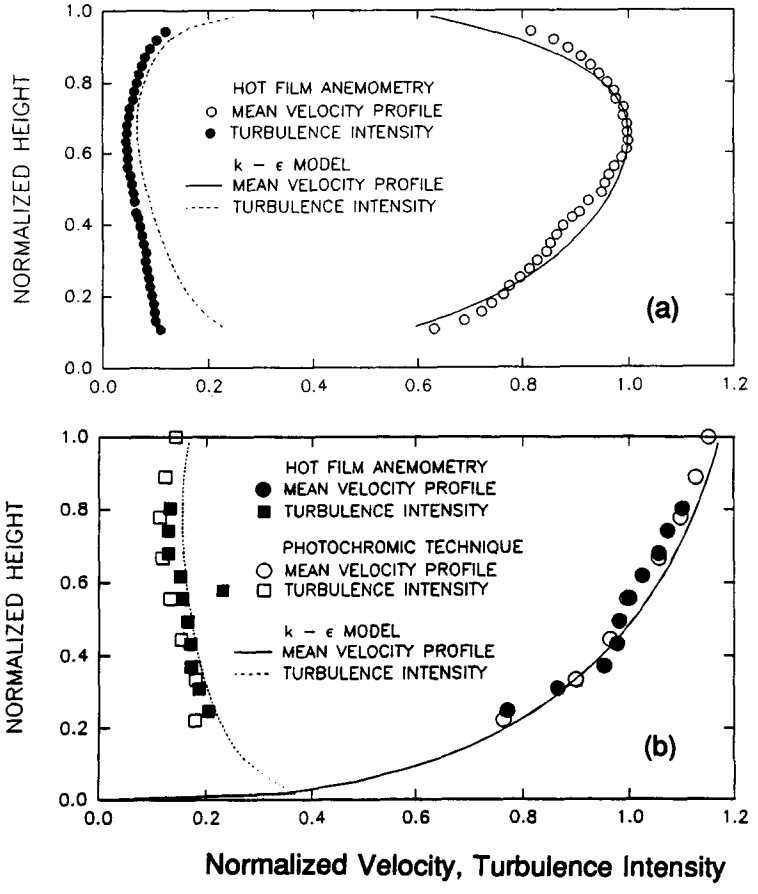

Figure 14. Normalized streamwise velocity and turbulence intensity profiles in cocurrent wavy-stratified flow (Run 200): (a) gas phase; and (b) liquid phase.

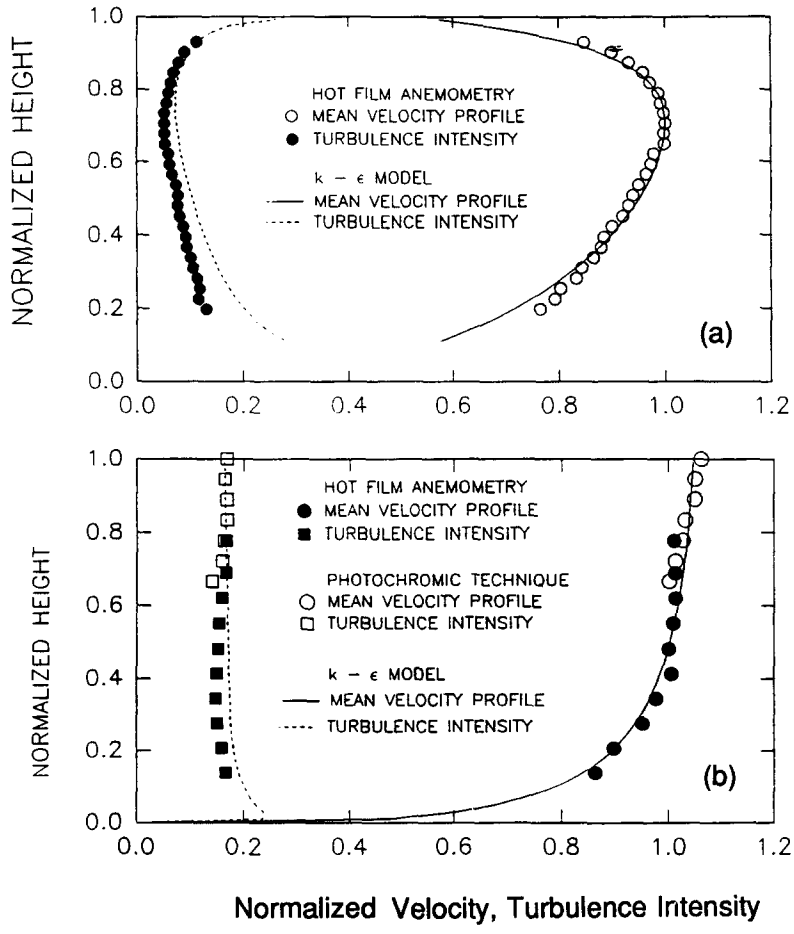

Figure 15. Normalized streamwise velocity and turbulence intensity profiles in cocurrent wavy-stratified flow (Run 300): (a) gas phase; and (b) liquid phase.

In all cases, an excellent agreement was seen among the numerical predictions and the experimental results obtained with HWA and PDA techniques. As seen from figures 14–17, the numerical velocity profiles predicted accurately the gas velocity profiles and the position of the plane of maximum velocity in the gas phase. Similarly, the flatness of the turbulent velocity profiles in the liquid phase were correctly reproduced. Although it seems that the levels of turbulence intensities were not accurately predicted, it is due to the fact that we did not measure the velocity fluctuations in the spanwise direction and therefore did not include the contribution of w′ in the measured TKE shown in figures 14–17. For turbulent open channel flows in a rectangular duct, Nalluri and Novak (1977), and for cocurrent flow, Fabre *et al.* (1983), quantitatively showed that the rms value of u' is the largest and that the magnitudes of v' and w' are nearly the same. Thus, it is not surprising that the numerical predictions tend to overestimate the data in both the liquid and gas phases in all cases of cocurrent and countercurrent flows. It is not certain whether w' would increase with the interfacial waviness in cocurrent and countercurrent flows as much as v' does, but most likely w' would remain relatively unchanged in magnitude while v' would increase much more significantly. Thus, the absence of w' in the measured TKE results should be of a lesser concern for the wavy flows shown in figures 14–17. The numerical predictions of the mean liquid height and pressure gradient matched the experimental results reasonably well, showing less than 15% difference, in all cases of cocurrent and countercurrent wavy-stratified flows.

Finally, it should also be pointed out that the TKE contribution, k_v, by itself was unable to predict the correct levels of turbulence in cocurrent and countercurrent flows, unlike in the study done by Akai *et al.* (1981) for air–mercury stratified flow. A possible explanation may be that the

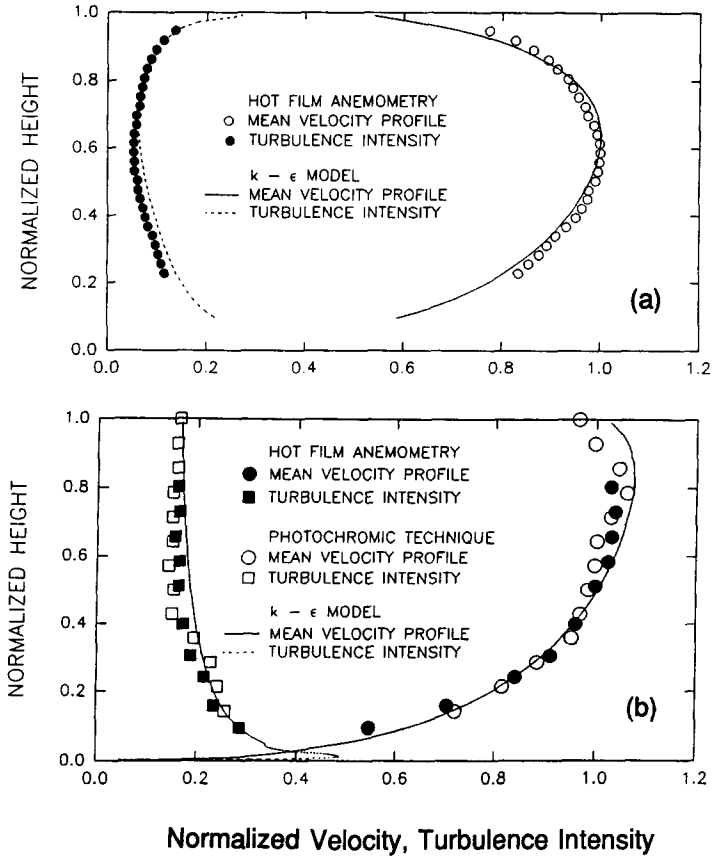

Figure 16. Normalized streamwise velocity and turbulence intensity profiles in countercurrent wavy-stratified flow (Run 400): (a) gas phase; and (b) liquid phase.

wave amplitudes in Akai *et al.*'s experiments were smaller, and consequently, a weaker gas–wave interaction was present. Thus, the k–ϵ model along with the interfacial conditions for the TKE as given by [13]–[15] and $\epsilon = k_L^{3/2}/ah_L$ for the dissipation rate, can be considered suitable for turbulent wavy-stratified flow with a shallow liquid layer. Deeper liquid streams such as in rivers and wind-wave tanks may require different boundary conditions for the wavy gas–liquid interface. In these cases, the liquid depth may not be an appropriate characteristic length for ϵ.

5. CONCLUSIONS

Hot film anemometry and a non-intrusive photochromic dye activation technique were used to study an open channel flow, and cocurrent and countercurrent stratified two-phase flows with a wavy interface. By overlapping the experimental results obtained with both techniques, a detailed description of the kinematic and turbulence fields of the liquid phase near and at the gas–liquid interface was obtained, overcoming limitations encountered in previous studies using techniques such as LDA.

The presence of interfacial shear and waves changed significantly the kinematic and turbulence structures of the liquid phase in the neighborhood of the wavy gas–liquid interface as compared to open channel flows with a smooth liquid surface. The streamwise velocity fluctuations were observed to be enhanced primarily by the intense shearing in the upper layers of the liquid, while the increase in magnitude of the vertical fluctuations was associated mostly with the increase in interfacial wave amplitude. The strong interaction between the gas flow and the waves created interfacial turbulent bursts that increased considerably the mixing in the upper layers of the liquid.

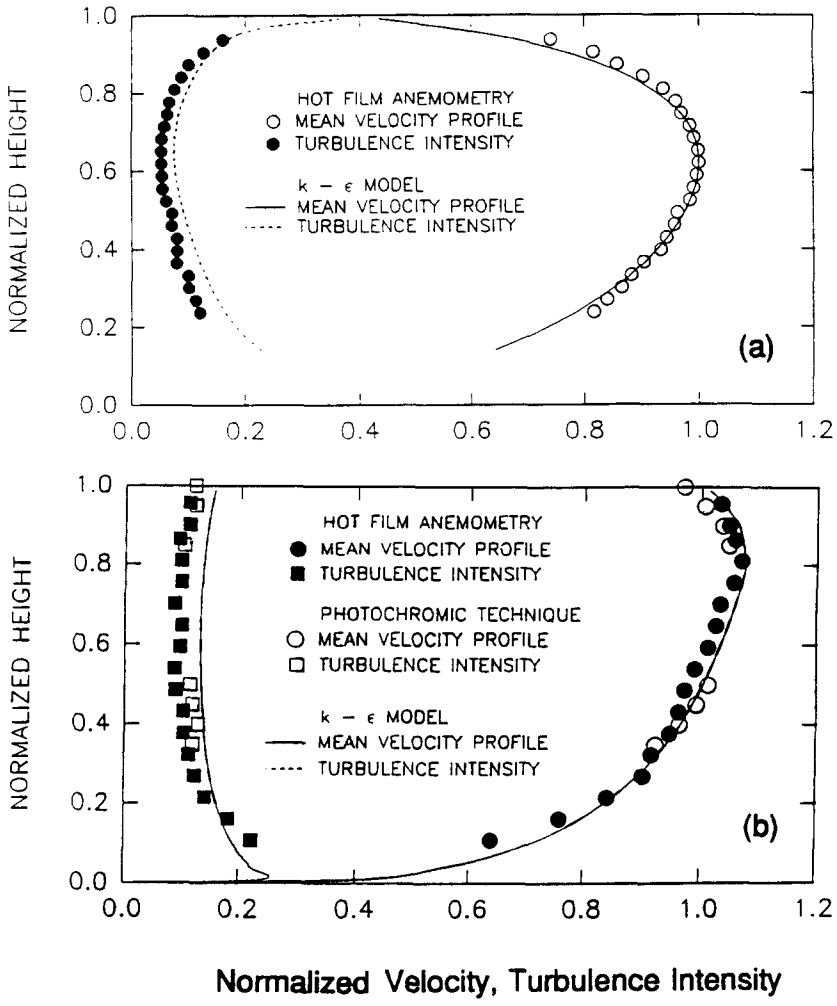

Figure 17. Normalized streamwise velocity and turbulence intensity profiles in countercurrent wavy-stratified flow (Run 500): (a) gas phase; and (b) liquid phase.

In consequence, the Reynolds stress profiles were considerably modified as compared to the linear profile of open channel flow.

Assuming that the convection provided by secondary flow is negligible, a new interfacial boundary condition for the turbulence kinetic energy to be used with the k–ϵ model for wavy–stratified flows was proposed, in which the contributions from the interfacial shear and wave motion to the turbulence kinetic energy are separately considered. Numerical predictions using the interfacial condition produced satisfactory results for both cocurrent and countercurrent wavy–stratified flows.

Acknowledgements—This work was supported by the Natural Science and Engineering Research Council of Canada and the Japan Atomic Energy Research Institute. The scholarship awarded by Isfahan University of Technology in Iran to M. Nasr-Esfahany is also gratefully acknowledged.

REFERENCES

Akai, M., Inoue, A. and Aoki, S. (1981) The prediction of stratified two-phase flow with a two-equation model of turbulence. *Int. J. Multiphase Flow* **7**, 21–39.

Benkirane, R., Line, A. and Masbernat, L. (1990) Modeling of wavy stratified flow in a rectangular channel. In *Phase–Interface Phenomena in Multiphase Flow*, eds G. F. Hewitt, F. Mayinger and J. R. Riznic, pp. 121–128. Hemisphere, New York.

Celik, I. and Rodi, W. (1984) Simulation of free surface effects in turbulent channel flows. *Physico-Chem. Hydrodynam. J.* **5,** 217–227.

Fabre, J., Masbernat, L. and Suzanne, C. (1983) New results on the structure of stratified gas/liquid flow. In *Advances in Two-phase Flow and Heat Transfer*, eds S. Kakac and M. Ishii, Vol. 1, pp. 135–150. Martinus Nijhoff, The Hague.

Fabre, J., Masbernat, L. and Suzanne, C. (1987) Stratified flow, Part I: local structure. In *Multiphase Science and Technology*, Vol. 3, pp. 285–301. Hemisphere, Washington D. C.

Grass, A. J. (1971) Structural features of turbulent flow over smooth and rough boundaries. *J. Fluid Mech.* **50,** 233–246.

Hewitt, G. F. (1991) Phenomena in horizontal two-phase flows. *Proceedings of The International Conference on Multiphase Flow*, September 24–27, Tsukuba, Japan, pp. 1–10.

Hirano, S., Matsumoto, S., Tanaka, Y. and Yamamoto, T. (1989) Calibration of hot-film probes in water at low-velocities. In *Dantec Information* No. 8, pp. 11–15.

Humphrey, J. A. C. (1977) Effect of turbulence on the precision of velocity and velocity fluctuation data obtained by photochromic visualization. *Can. J. of Chem. Eng.* **55,** 126–130.

Iribarne, I., Frantisak, F., Hummel, R. L. and Smith, J. W. (1972) An experimental study of instabilities and other flow properties of a laminar pipe jet. *AIChE Journal* **18,** 689–697.

Issa, R. I. (1988) Predictions of turbulent, stratified, two-phase flow in inclined pipes and channels. *Int. J. Multiphase Flow* **14,** 141–154.

Johns, D. M., Theofanous, T. G. and Houze, R. N. (1975) Turbulent characteristics of two-phase, gas–liquid stratified channel flow. In *Proceedings of the Third Symposium on Turbulence in Liquids*, eds G. K. Patterson and J. L. Zakin, pp. 250–258.

Kawaji, M., Ahmad, W., DeJesus, J. M., Sutharshan B., Lorencez, C. and Ojha, M. (1993) Flow visualization of two-phase flows using photochromic dye activation method. *Nuclear Engineering and Design*, **141,** 343–355.

Kline, S. J., Reynolds, W. C., Schraub, F. A. and Runstadler, P. W. (1967) The structure of turbulent boundary layers. *J. Fluid Mech.* **30,** 741–758.

Kim, H. T., Kline, S. J. and Reynolds, W. C. (1971) The production of turbulence near a smooth wall in a turbulent boundary layer. *J. Fluid Mech.* **50,** 133–160.

Komori, S., Ueda, H., Ogino, F. and Mizushina, T. (1982) Turbulence structure and transport mechanism at the free surface in an open channel flow. *Int. J. Heat Mass Transfer* **25,** 513–521.

Komori, S., Hiraga, Y., Murakami, Y. and Ueda, H. (1988) The generation of surface renewal eddies in an open channel flows. In *Transport Phenomena in Turbulent Flows: Theory, Experiment and Numerical Simulation*, eds M. Hirata and N. Kasagi, pp. 213–216. Hemisphere, New York.

Komori, S., Murakami, Y. and Ueda, H. (1989) The relationship between surface-renewal and bursting motions in an open channel flow. *J. Fluid Mech.* **203,** 103–123.

Lorencez, C. (1994) Turbulent momentum transfer at a gas–liquid interface in horizontal stratified flow in a rectangular channel. Ph. D. thesis, Department of Chemical Engineering and Applied Chemistry, University of Toronto.

Lorencez, C., Chang, T. and Kawaji, M. (1991) Investigation of turbulent momentum transfer at a gas–liquid interface in a horizontal countercurrent stratified flow. In *Turbulence Modification in Multiphase Flows, Proc. 1st ASME/JSME Fluids Eng. Conf.*, Portland, OR, ASME-FED, Vol. 110, pp. 97–102.

Lorencez, C., Kawaji, M., Ojha, M., Ousaka, A. and Murao, Y. (1993) Application of a photochromic dye activation method to stratified flow with smooth and wavy gas–liquid interface. *ANS Proc. of National Heat Transfer Conference*, Atlanta, GA. HTC-Vol. 7, pp. 160–168.

Murata, A., Hihara, E. and Saito, T. (1991) Turbulence below an air-water interface in a horizontal channel. In *Turbulence Modification in Multiphase Flows, Proc. 1st ASME/JSME Fluids Eng. Conf.*, Portland, OR, ASME-FED, Vol. 110, pp. 67–74.

Nakagawa, H. and Nezu, I. (1981) Structure of space-time correlation of bursting phenomena in an open channel flow. *J. Fluid Mech.* **104,** 1–14.

Nalluri, C. and Novak, P. (1977) Turbulence characteristics in open channel flow. *Proc. of the Fifth Biennial Symposium on Turbulence*, October, 1977, eds G. K. Patterson and J. L. Zakin, pp. 191–204. Science Press, Princeton.

Nezu, I and Rodi, W. (1986) Open channel flow measurements with a laser Doppler anemometer. *J. Hydraulic Engng* **112,** 335–335.

Ojha, M., Hummel, R. L., Cobbold, R. S. and Johnston, K. W. (1988) Development and evaluation of a high resolution photochromic dye method for pulsatile flow studies. *J. Phys. E. Sci. Instrum.* **21,** 998–1004.

Patankar, S. V. (1980) *Numerical Heat Transfer and Fluid Flow*. McGraw-Hill, New York.

Popovich, A. T. and Hummel, R. L. (1967) A new method for non-disturbing turbulent flow measurements very close to a wall. *Chem. Eng. Sci.* **22,** 21–29.

Rashidi, M. and Banerjee, S. (1990) Streak characteristics and behavior near wall and interface in open channel flows. *ASME J. Fluids Engng* **112,** 164–170.

Rashidi, M., Hetsroni, G. and Banerjee, S. (1992) Wave-turbulence interaction in free-surface channel flows. *Phys. Fluids A.* **4,** 2727–2738.

Sadatomi, M., Kawaji, M., Lorencez, C. and Chang, T. (1993) Prediction of liquid level distribution in horizontal gas-liquid flows with interfacial level gradient. *Int. J. Multiphase Flow* **19,** 987–997.

Seeley, L. E., Hummel, R. L. and Smith, J. W. (1975) Experimental velocity profiles in laminar flow around spheres at intermediate Reynolds numbers. *J. Fluid Mech.* **68,** 591–598.

Smith, C. R. and Metzler, S. P. (1983) The characteristics of low-speed streaks in the near wall region of a turbulent boundary layer. *J. Fluid Mech.* **129,** 27–45.